Journal of Earth Science, *Vol. 27*, *No. 5*, *p. 727–739*, *October 2016* *ISSN 1674-487X*
Printed in China
DOI: 10.1007/s12583-016-0701-9

Effects of Crustal Eclogitization on Plate Subduction/Collision Dynamics: Implications for India-Asia Collision

Pengpeng Huangfu[1, 2, 3], **Yuejun Wang**[3, 4], **Zhonghai Li**[2], **Weiming Fan**[4], **Yan Zhang***[3]

1. *State Key Laboratory of Isotope Geochemistry*, *Guangzhou Institute of Geochemistry*, *Chinese Academy of Sciences*, *Guangzhou* 510640, *China*
2. *Key Laboratory of Computational Geodynamics*, *College of Earth Sciences*, *University of Chinese Academy of Sciences*, *Beijing* 100049, *China*
3. *School of Earth Science and Geological Engineering*, *Sun Yat-Sen University*, *Guangzhou* 510275, *China*
4. *CAS Center for Excellence in Tibetan Plateau Earth Sciences*, *Key Laboratory of Continental Collision and Plateau Uplift*, *Institute of Tibetan Plateau Research*, *Chinese Academy of Sciences*, *Beijing* 100101, *China*

ABSTRACT: 2D thermo-mechanical models are constructed to investigate the effects of oceanic and continental crustal eclogitization on plate dynamics at three successive stages of oceanic subduction, slab breakoff, and continental subduction. Crustal eclogitization directly increases the average slab density and accordingly the slab pull force, which makes the slab subduct deeply and steeply. Numerical results demonstrate that the duration time from initial continental collision to slab breakoff largely depends on the slab pull force. Specifically, eclogitization of subducted crust can greatly decrease the duration time, but increase the breakoff depth. The detachment of oceanic slab from the pro-continental lithosphere is accompanied with obvious exhumation of the subducted continental crust and a sharp uplift of the collision zone in response to the disappearance of downward drag force and the induced asthenospheric upwelling, especially under the condition of no or incomplete crustal eclogitization. During continental subduction, the slab dip angle is strongly correlated with eclogitization of subducted continental lower crust, which regulates the slab buoyancy nature. Our model results can provide several important implications for the Himalayan-Tibetan collision zone. For example, it is possible that the lateral variations in the degree of eclogitization of the subducted Indian crust might to some extent contribute to the lateral variations of subduction angle along the Himalayan orogenic belt. Moreover, the accumulation of highly radiogenic sediments and upper continental crustal materials at the active margin in combination with the strong shear heating due to continuous continental subduction together cause rising of isotherms in the accretionary wedge, which facilitate the development of crustal partial melting and metamorphism.

KEY WORDS: numerical modeling, crustal eclogitization, oceanic subduction, slab breakoff, continental subduction, Himalayan-Tibetan collision zone.

0 INTRODUCTION

The slab pull is generally believed to be the driving mechanism for plate subduction (e.g., Schellart, 2004; Lithgow-Bertelloni and Richards, 1995; Vigny et al., 1991; Forsyth and Uyeda, 1975). From the mechanical perspective, eclogitization of subducted mafic crust increases the average slab density and accordingly the slab pull force, which thereby exerts an effect on the geodynamic processes (e.g., Duesterhoeft et al., 2014; van Hunen et al., 2004, 2001; Leech, 2001). Eclogitization usually takes place in subducted slab in the subduction zone or in the thickened continental lower crust within the collisional zone (Leech, 2001).

During oceanic subduction, slab dynamics, especially the slab dip variability, can be to first order attributed to a balance between the gravitational and hydrodynamic torques (Manea et al., 2006; Stevenson and Turner, 1977). Any factor that can change either torque can exert an effect on the slab geodynamic process. Eclogitization of the subducted oceanic crust, by virtue of increasing the gravitational torque, can regulate the slab geometry. The influence of the basalt-to-eclogite transformation rate on the formation of flat subduction was investigated with numerical modeling (van Hunen et al., 2004, 2001). The influence of eclogitization of continental lower crust is also evaluated in previous works (e.g., Lustrino, 2005; Leech, 2001). However, these researches mostly focus on the delamination/detachment of lower crust with the subjacent lithospheric mantle in the thickened continental collision zone, and effects of crustal eclogitization during continental subduction have been poorly investigated.

*Corresponding author: shanshizhang@sohu.com

Manuscript received July 28, 2015.
Manuscript accepted April 26, 2016.

Huangfu, P. P., Wang, Y. J., Li, Z. H., et al., 2016. Effects of Crustal Eclogitization on Plate Subduction/Collision Dynamics: Implications for India-Asia Collision. *Journal of Earth Science*, 27(5): 727–739. doi:10.1007/s12583-016-0701-9. http://en.earth-science.net

Continental subduction naturally follows oceanic subduction under the lateral ridge push and/or slab pull (Li et al., 2011). We can evaluate the eclogitization of both subducted oceanic crust and continental lower crust in a model, which begins with oceanic subduction and ends with continental subduction. In this study, the sensitivity tests of model predictions to the crustal eclogitization, using 2D thermo-mechanical numerical modeling, are performed. The numerical results are also compared with the Himalayan-Tibetan collision zone, attempting to provide implications for the tectonic evolution at the early stage of India-Asia collision.

1 MODEL CONFIGURATION

1.1 Numerical Code Description

1.1.1 Principal equations

The finite difference method combined with the marker-in-cell technique is implemented in the algorithm proposed by Gerya (2010). Principal equations include momentum equation, incompressible continuity equation and heat conversation equation, accounting for the 2D thermal creeping flows containing chemical buoyant and thermal forces. All abbreviations and units used are listed in Table 1.

(1) 2D stokes equations

$$\frac{\partial \sigma'_{xx}}{\partial \mathrm{x}}+\frac{\partial \sigma'_{xz}}{\partial z}=\frac{\partial P}{\partial x}$$

$$\frac{\partial \sigma'_{zx}}{\partial \mathrm{x}}+\frac{\partial \sigma'_{zz}}{\partial \mathrm{z}}=\frac{\partial P}{\partial z}-g\rho\left(C,M,P,T\right) \tag{1}$$

where the density ρ depends on composition (C), melt fraction (M), temperature (T), and pressure (P).

(2) Incompressible continuity equation

$$\frac{\partial v_x}{\partial \mathrm{x}}+\frac{\partial v_z}{\partial z}=0 \tag{2}$$

(3) Heat conservation equations

$$\rho C_p\left(\frac{DT}{Dt}\right)=-\frac{\partial q_x}{\partial x}-\frac{\partial q_z}{\partial z}+H_r+H_a+H_s$$

$$q_x=-k\left(T,P,C\right)\frac{\partial T}{\partial x}\quad q_z=-k\left(T,P,C\right)\frac{\partial T}{\partial z} \tag{3}$$

$$H_a=\mathrm{T}\alpha\frac{dP}{dt}\quad H_s=\sigma'_{xx}\dot{\varepsilon}_{xx}+\sigma'_{zz}\dot{\varepsilon}_{zz}+2\sigma'_{xz}\dot{\varepsilon}_{xz}$$

where DT/Dt and $k(T, P, \mathrm{c})$ mean the substantive time derivative of temperature and the thermal conductivity dependent on temperature, pressure and composition (Clauser and Huenges, 1995); H_r, H_a and H_s refer to radioactive heat production, energetic effect of isothermal compression/decompression (i.e., adiabatic heating/cooling), and shear heating, respectively.

1.1.2 Rheological model

The visco-plastic constitute laws are used to demonstrate the correlation of the deviatoric stress (σ'_{ij}) with the strain rate tenser ($\dot{\varepsilon}_{xx}$). In terms of incompressible viscous deformation, the viscous laws of friction can be expressed as

$$\sigma'_{xx}=2\eta_{eff}\dot{\varepsilon}_{xx}\quad \dot{\varepsilon}_{xx}=\frac{\partial v_x}{\partial x}$$

$$\sigma'_{xz}=2\eta_{eff}\dot{\varepsilon}_{xz}\quad \dot{\varepsilon}_{xz}=\frac{1}{2}\left(\frac{\partial v_x}{\partial z}+\frac{\partial v_z}{\partial x}\right) \tag{4}$$

$$\sigma'_{zz}=2\eta_{eff}\dot{\varepsilon}_{zz}\quad \dot{\varepsilon}_{zz}=\frac{\partial v_z}{\partial z}$$

where η_{eff} notes the effective viscosity determined by temperature, pressure, composition and strain rate.

The effective viscosity for ductile creep is described as

$$\eta_{ductile}=\left(\dot{\varepsilon}_{II}\right)^{\frac{1-n}{n}}F\left(A_D\right)^{-\frac{1}{n}}\exp\left(\frac{E+PV}{nRT}\right) \tag{5}$$

where $\dot{\varepsilon}_{II}=\left(0.5\dot{\varepsilon}_{ij}\dot{\varepsilon}_{ij}\right)^{1/2}$ is the second invariant of the rate of strain tensor and A_D, E, n and V denote parameters for flow low (Table 2). F is related with the experiment type, specifically, $F=2^{(1-\mathrm{n})/\mathrm{n}}$ for simple shear test and $F=2^{(1-\mathrm{n})/\mathrm{n}}/3^{(1+\mathrm{n})/2\mathrm{n}}$ for triaxial compression test.

The plastic yielding stress is obtained based on the Mohr-Coulomb criterion

$$\sigma_{yield}=C_0+\mathrm{P}\sin\left(\varphi_{\mathrm{eff}}\right)$$

$$\sin\left(\varphi_{eff}\right)=\sin\left(\varphi\right)\left(1-\lambda\right) \tag{6}$$

where σ_{yield} is the yield stress, C_0 is the cohesion and φ is the internal frictional angle; P is the dynamic pressure; λ is the pore fluid coefficient.

1.1.3 Eclogitization

From the mechanical perspective, crustal eclogitization affects the plate dynamics by virtue of increasing the slab average density and accordingly the slab pull force. Generally, eclogitization takes place in subducted oceanic crust and continental lower crust and in the thickened continental lower crust within the collisional orogenic zone (Leech, 2001), where the required pressure-temperature conditions, as shown in Fig. 1, can be satisfied. Based on pressure-temperature conditions for stable metamorphic facies (Fig. 1), the transformation from basalt/gabbro to eclogite commonly commences at a depth of ~50 km. After crustal eclogitization, the buoyancy nature of the subducting slab can be changed, which is generally described by the theory of Riedell and Karato (1996). Giunchi and Ricard (1999) proposed another simplified numerical equation for this transformation. In this study, the crustal eclogitization is simplified as a process of density increase of the subducted crustal materials depending on the sinking depth, and the maximum density of these crustal materials is equal to the density of eclogite (3 500 kg/m^3, used in this study). Specifically, density of the subducted crustal materials during eclogitization, ρ_{ec}, is linearly computed using the following equation

$$\rho_{ec}=\frac{d-d_{ini}}{50}\left(3500-\rho_{oc}^0\right)+\rho_{oc}^0\quad (50\ \mathrm{km}\le d\le 100\ \mathrm{km})$$

$$\rho_{ec}=3500,\ (100\ \mathrm{km}\le d) \tag{7}$$

where d is depth of subducted oceanic crust or continental

lower crust; d_{ini} is initial depth, where eclogitization of subducted crust begins (50 km, herein used); ρ_{oc}^{0} is original crust density free of eclogitization.

1.2 Initial Model Setup

Large scale numerical models (2 800×1 400 km, Fig. 2) were constructed to evaluate the affects of crustal eclogitization on plate dynamics. The model is made up of a non-uniform 251×76 rectangular grid with a variable resolution from 3×3 km around the subduction zone to becoming larger gradually further away. Meanwhile, ~0.6 million active Lagrangian markers with various rock properties are distributed in the computational domain. Mechanical parameters of various rocks are illustrated in Table 2, which can account for brittle and ductile deformation of crustal and mantle rocks.

Table 1 Notations and units of the variables for the numerical experiment

Symbols	Meaning	Units
A_D	Material constant	$MPa^{-n}\cdot s^{-1}$
C	Composition	Dimensionless
C_0	Cohesion	MPa
Cp	Isobaric heat capacity	$J\cdot K^{-1}\cdot kg^{-1}$
E	Activation energy	$kJ\cdot mol^{-1}$
F	Power law viscous rheology coefficient	Dimensionless
g	Gravitational acceleration	$m\cdot s^{-2}$
G	Plastic potential	Pa
H_a, H_r, H_s, H_L	Adiabatic, radioactive, shear and latent heat production	$W\cdot m^{-3}$
k	Thermal conductivity	$W\cdot m^{-1}\cdot K^{-1}$
M	Melt fraction	Dimensionless
N	Stress exponent	Dimensionless
P	Dynamic pressure	Pa
P_{fluid}	Pore fluid pressure	Pa
P_{lith}	Lithostatic pressure	Pa
q_x, q_z	Horizontal and vertical heat fluxes	$W\cdot m^{-2}$
Q_L	Latent heat of melting	$kJ\cdot kg^{-1}$
R	Gas constant	$J\cdot K^{-1}\cdot mol^{-1}$
t	Time	s
T	Temperature	K
V	Activation volume	$J\cdot MPa^{-1}\cdot mol^{-1}$
α	Thermal expansion coefficient	K^{-1}
β	Compressibility coefficient	Pa^{-1}
$\dot{\varepsilon}_{ij}$	Components of the strain rate tensor	s^{-1}
$\dot{\varepsilon}_{II}$	Second invariant of the strain rate tensor	s^{-1}
η	Viscosity	Pa·s
λ	Pore fluid pressure coefficient	Dimensionless
ρ	Density	$kg\cdot m^{-3}$
$\dot{\sigma}_{ij}$	Components of the viscous deviatoric stress tensor	Pa
$\dot{\sigma}_{II}$	Second invariant of the stress tensor	Pa
σ_{yield}	Yield stress	Pa
φ	Internal frictional angle	Rad

Our numerical model comprises three major domains, consistent with the general considerations (see Li, 2014 for a review), involving (1) a pro-continental domain (1 000 km long), (2) an oceanic domain (500 km long), and (3) a retro-continental domain (1 300 km long), as shown in Fig. 2. The 103 km thick continental lithospheres in both continental domains are composed of 6 km thick sediments, 14 km thick upper crust, 15 km thick lower crust and 68 km thick mantle lithosphere. The oceanic domain comprises 76 km thick oceanic lithosphere (containing 2 km thick oceanic upper crust and 5 km thick oceanic lower crust) and subjacent asthenospheric mantle. The spontaneous deformation of the lithospheric surface acting as a weak top-layer is regarded as an internal free surface, which is dynamically calculated at each step (Gerya and Yuen, 2003). A weak zone, which is represented by materials with low plastic strength and weak rheological properties (wet olivine flow law (Ranalli, 1995)), is intentionally set to facilitate initial oceanic subduction in the right ocean-continent transition zone. This initial weak zone cuts through the whole lithosphere with a dip angle of 27°.

All boundaries in this model satisfy the free-slip conditions. The pushing velocity is assigned to a small internal domain within the pro-continental lithosphere, but is changed during computation. Specifically, a pushing velocity of 10 cm/yr is set during the oceanic subduction. Then, from the initial continental collision to the oceanic slab breakoff, the pushing velocity is cancelled, and the geodynamic processes are only driven by slab pull. Afterwards, in order to further study the post-collision evolution, we use the end result of oceanic slab breakoff as the starting situation with a pushing velocity of 4 cm/yr for the subsequent continental subduction/collision.

The initial thermal structure of continental lithosphere is linearly increases from 0 °C at the surface to 1 200 °C at the bottom of the lithospheric mantle. The initial thermal structure of oceanic lithosphere is set according to the oceanic plate cooling model with an age of 40 Ma (Turcotte and Schubert, 2002). An initial temperature gradient of 0.5 °C/km is assigned to the sub-lithospheric mantle.

2 NUMERICAL RESULTS

The sensitivity tests of model predictions to crustal eclogitization are evaluated. Numerical models without or with eclogitization of subducted oceanic crust and continental lower crust are investigated at three successive stages involving oceanic subduction, slab breakoff and continental subduction.

2.1 Model without Crustal Eclogitization

2.1.1 Oceanic subduction and initial continental collision

During oceanic subduction, the first order control on slab dynamics can be attributed to a balance of driving forces and resisting forces (e.g., Stevenson and Turner, 1977). The slab pull force, regarded as the main driving force, is also believed as a driving mechanism for plate tectonics (Schellart, 2004). Deformation behaviour of the overriding plate is controlled by the dynamic equilibrium of the slab pull that draws the overriding plate downward with the interplate buoyant force

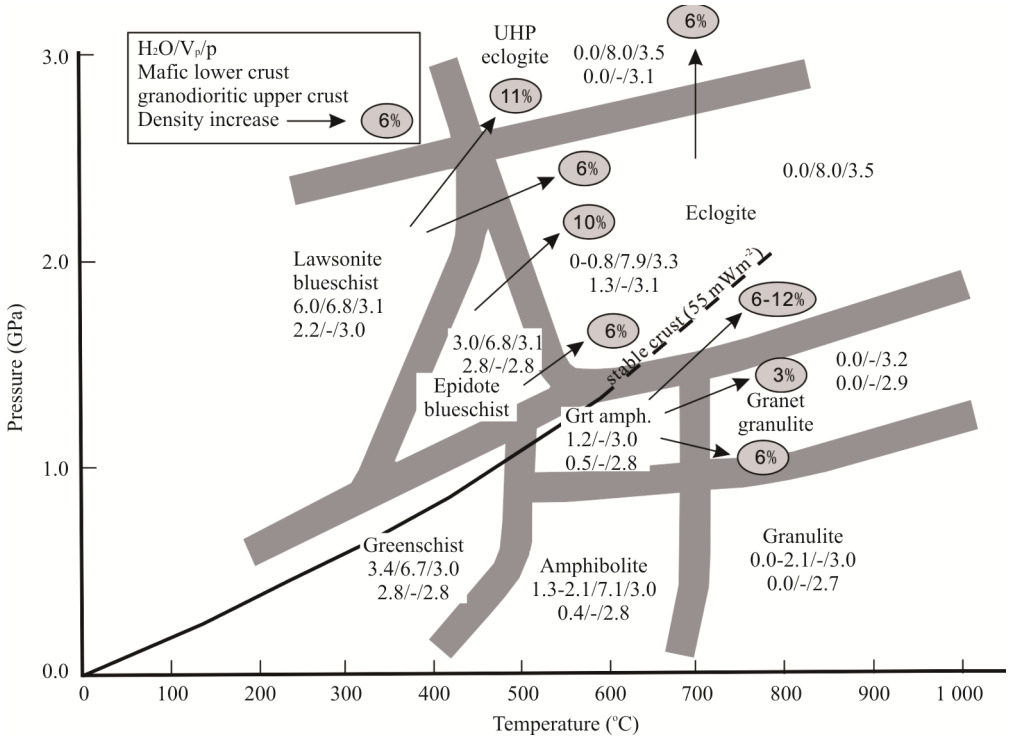

Figure 1. Stable metamorphic facies with regard to temperature and pressure (Leech, 2001). Averages estimated maximum fluid contents (vol%), seismic velocities ($km \cdot s^{-1}$) and densities ($g \cdot cm^{-3}$) for granodioritic and basaltic compositions are contained to display buoyancy and H_2O relationship. Arrows show density increase accompanying various metamorphic transformations. Conductive temperature profiles of the Sierra Nevada and the basin and range are also shown.

Table 2 Materials properties used in 2-D numerical experiments

Material	ρ_0 ($kg \cdot m^{-3}$)	k ($W \cdot m^{-1} K^{-1}$)	H_r ($\mu W \cdot m^{-3}$)	Flow law	E ($kJ \cdot mol^{-1}$)	n	A_D ($MPa^{-n} \cdot s^{-1}$)	V ($J \cdot MPa^{-1} \cdot mol^{-1}$)	sin(φ)	C (GPa)
Sediments	2 700	$0.64+\frac{807}{T+77}$	2.0	Wet quartzite	154	2.3	3.2×10^{-4}	0	0.03	10
Upper continental crust	2 700	$0.64+\frac{807}{T+77}$	1.0	Wet quartzite	154	2.3	3.2×10^{-4}	8	0.15	10
Lower continental crust	2 900	$1.18+\frac{474}{T+77}$	0.25	Plagioclase	238	3.2	3.3×10^{-4}	12	0.15	25
Upper oceanic crust	3 100	$0.64+\frac{807}{T+77}$	0.25	Wet quartzite	154	2.3	3.2×10^{-4}	8	0.3	25
Lower oceanic crust	3 100	$1.18+\frac{474}{T+77}$	0.25	Plagioclase	238	3.2	3.3×10^{-4}	8	0.6	25
Continental lithospheric mantle	3 350	$0.73+\frac{1293}{T+77}$	0.022	Dry olivine	532	3.5	2.5×10^{4}	10	0.6	67
Oceanic lithospheric mantle	3 370	$0.73+\frac{1293}{T+77}$	0.022	Dry olivine	532	3.5	2.5×10^{4}	12	0.6	67
Asthenosphere	3 350	$0.73+\frac{1293}{T+77}$	0.022	Dry olivine	532	3.5	2.5×10^{4}	10	0.6	67
Weak zone	3 200	$0.73+\frac{1293}{T+77}$	0.022	Wet olivine	137	1.9	2.0×10^{-4}	0	0.03	67
Reference[a]	1	2	3	4	4	4	4	4	4	3

[a]. 1. Bittner and Schmeling (1995); 2. Clauser and Huenges (1995); 3. Turcotte and Schubert (2002); 4. Ranalli (1995).

(Jischke, 1975). After subduction initiation, the subduction angle gradually increases from 26° to ~50° (Fig. 3), by virtue of slab pull resulting from the density contrast induced by temperature difference between the slab and the surrounding asthenospheric mantle. Both frontal and basal subduction erosion can be observed. The former is confirmed by the presence of sediments and continental crustal materials in the subduction channel eroded off the overriding continent surface (Figs. 3b and 3c). The latter is correlated with the obvious downward migration and erosion of the overriding lithospheric mantle adjacent to the slab upper surface (Fig. 3c).

After the termination of oceanic subduction at 6.6 Myr, the pushing velocity assigned to the pro-continental plate is cancelled and the subsequent geodynamic process at this stage is

only driven by slab pull. However, without crustal eclogitization, the average density of the slab is relatively small, which accordingly results in a rather long duration time of ~25 Myrs (Fig. 4) and a shallow depth of ~200 km for slab breakoff (Fig. 4d). Specifically, because of deficiency in slab pull force, a long duration time is required to sufficiently weaken the slab, especially the ocean-continent transitional zone, through thermal conduction heating. In combination with the buoyant nature of the continental lithosphere without lower-crust eclogitization, the pro-continental plate cannot continuously slide into the asthenospheric mantle, which eventually causes the oceanic slab to detach from the continental plate at a depth of ~200 km. In addition, this stage is also characterized by the large-scale exhumation of the subducted continental crust and strong upwelling of the hot asthenospheric materials through the gap between two plates (Fig. 4). Exhumation process of the subducted crustal materials can be divided into three stages: (1) detachment of sediments from the upper crust and ascending to the surface first (Fig. 4b), (2) detachment of upper crustal materials from the lower crust and ascending upward at a larger depth (Fig. 4c), (3) and eventually detachment of lower crustal materials from the subjacent lithospheric mantle at a asthenospheric depth (Fig. 4d). Such exhumation processes are similar to that in Zheng et al. (2013).

2.1.2 Post-collisional evolution

After detachment of the oceanic slab and resuming assigning a pushing velocity of 4 cm/yr to the pro-continental plate, active continental collision commences, which is treated as the onset of the "hard collision" between two convergent continental plates. During continental subduction, most sediment materials are scraped off the downgoing pro-continental plate, and accumulate in the accretionary wedge (Fig. 5a). The bulk of crustal materials can slide into the asthenosphere with the subjacent lithospheric mantle (Fig. 5b). Subsequently, the subduction angle gradually decreases in correlation with an increasing amount of the buoyant continental crust entering the asthenosphere (Figs. 5c and 5d). At the same time, some subducted crustal materials begin to detach from the slab and move up vertically until they collapse at the bottom of the overriding lithospheric mantle (Figs. 5c and 5d). The continuous underthrusting of the pro-continental lithosphere with a low subduction angle makes hot asthenospheric materials squeezed out and replaced by the relatively cold continental slab, restraining the development of the large-scale magmatism within the overriding plate. However, the accumulation of highly radiogenic sediments materials accompanying strong shear heating due to continuous continental subduction favors rising of isotherms in the accretionary wedge (Fig. 5d), which can greatly facilitate the development of crustal partial melting and thermal metamorphism in this orogenic zone.

2.2 Model with Crustal Eclogitization

Except that crustal eclogitization is involved, all the other parameters of this model remain identical to that of the above model.

2.2.1 Oceanic subduction and initial continental collision

After subduction initiation, the slab dip angle gradually increases from 26° to ~65° (Fig. 6), resulting from the increasing

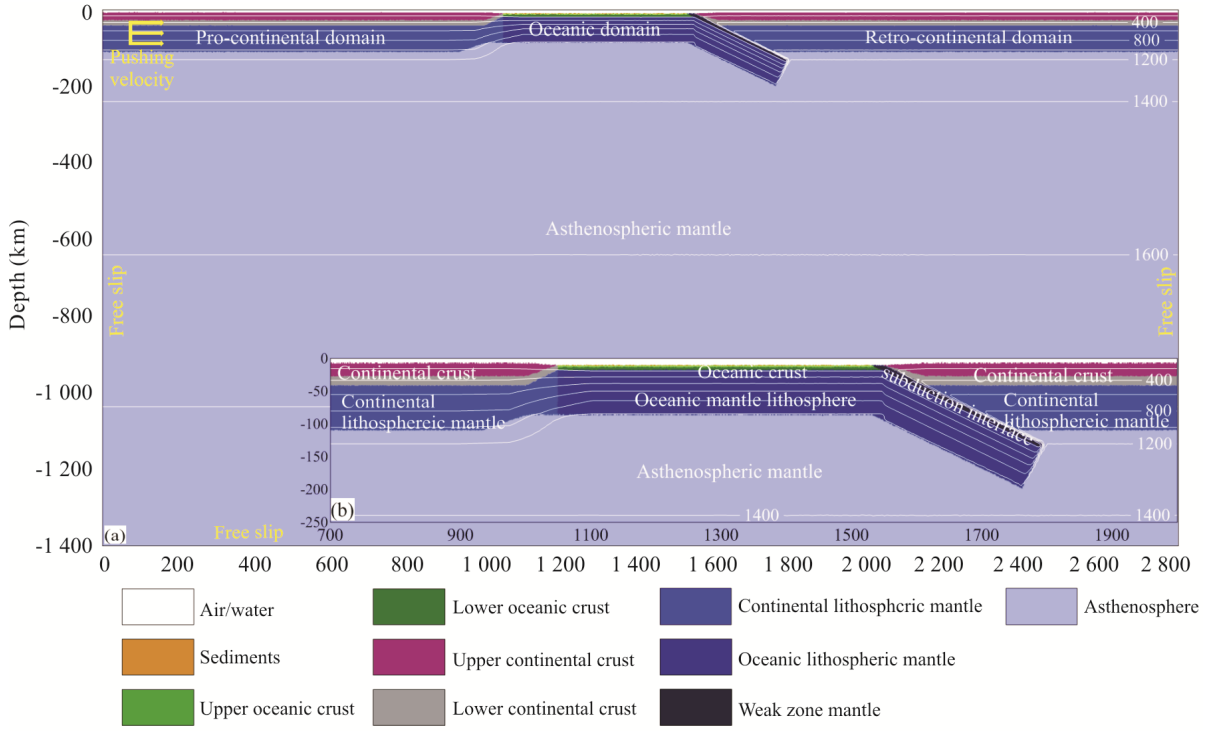

Figure 2. Initial setup of numerical modeling in this study. (a) Initial model configuration with temperature (isotherms in °C) and boundary conditions (in yellow). (b) The zoomed domain illustrating the initial structure of the subduction zone. A weak zone is prescribed in the mantle lithosphere to initiate the continental subduction.

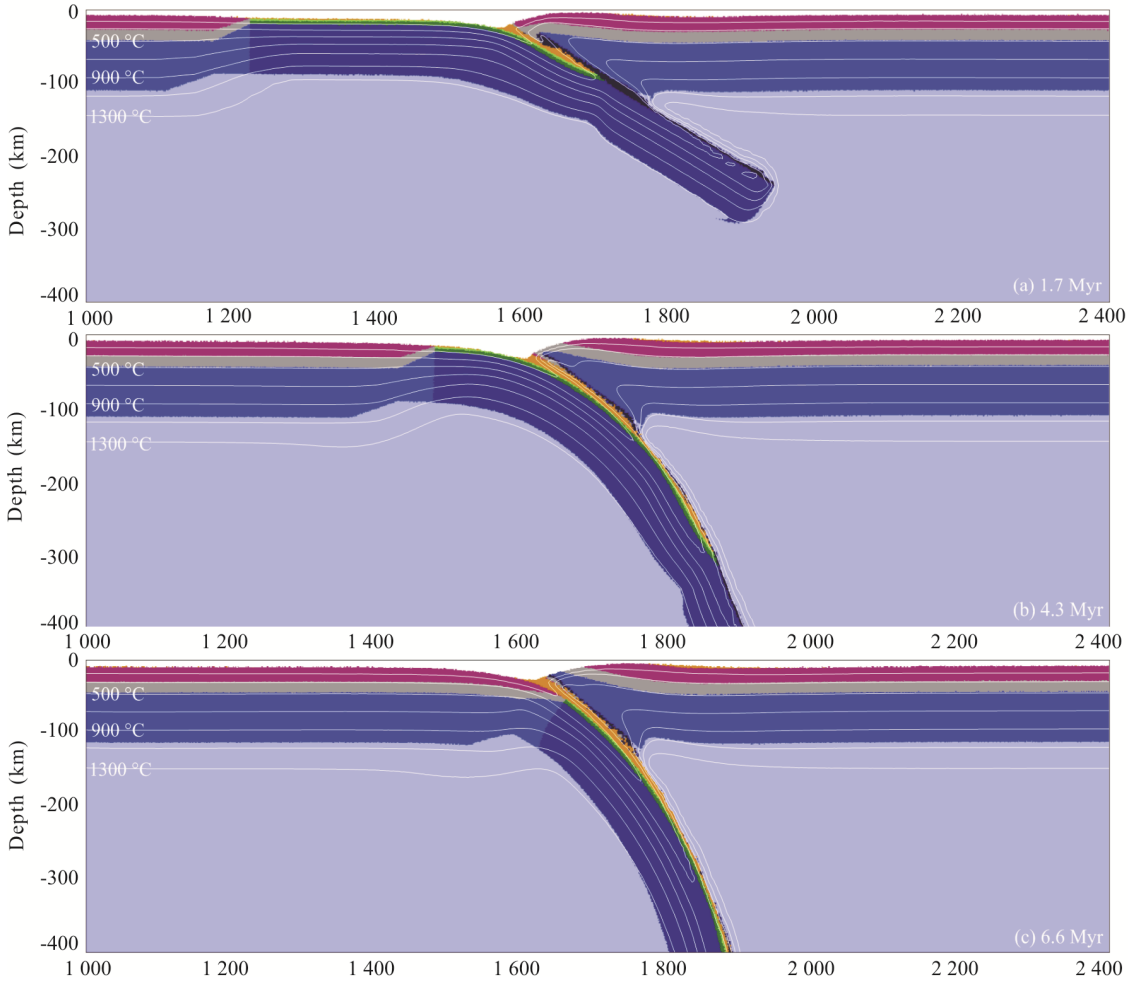

Figure 3. Evolution of the model without crustal eclogitization during oceanic subduction at time of (a) 1.7 Myr, (b) 4.3 Myr and (c) 6.6 Myr within an enlarged 1 400×400 km domain of the initial 2 800×1 400 km model. Colors of rocks are identical to those in Fig. 2. While numbered lines are isotherms in °C.

slab pull force due to eclogitization of the subducted oceanic crust. Both frontal and basal subduction erosion can be observed during oceanic subduction, which are separately correlated with the presence of continental crustal materials in the subduction channel eroded off the fore-arc wedge surface (Figs. 6b and 6c) and the obvious downward migration and erosion of the overriding lithospheric mantle adjacent to the slab upper surface (Fig. 6c). The closure of the ocean basin, as shown in Fig. 6c, indicates the termination of oceanic subduction and the commencement of continental collision.

In contrast to the model without crust eclogitization, the pro-continental plate still undergoes continuous subduction after the termination of oceanic subduction at 5.4 Myr, driven by the increasing slab pull due to eclogitization of subducted oceanic crust. Some continental crustal materials can be dragged to sink to a depth of >200 km (Figs. 7a and 7b). Subsequently, the opposing buoyancy forces, resulting from the dense oceanic slab and buoyant continental lithosphere, lead to extensional deformation in the ocean-continent transitional zone, which therefore induces a narrow rifting at 8.9 Myr (Fig. 7b) and eventually causes slab breakoff at a depth of ~300 km at 11.5 Myr (Fig. 7c). The slab breakoff instantly triggers asthenosphere upwelling beneath the collision zone, impinging on the overriding lithospheric mantle. The resultant thermal perturbation is potentially able to lead to large-scale partial melting of the subducted continental crust in the subduction channel.

2.2.2 Post-collisional evolution

In order to investigate the effects of crustal eclogitization on the continental collision process, the end result of the oceanic slab breakoff is used as the starting model but with a convergence velocity of 4 cm/yr assigned to the pro-continental lithosphere. Eclogitization of the subducted continental lower crust increases the average density of the continental slab and exerts a negative buoyancy force on the slab, which therefore causes the pro-continental lithosphere to sink to a greater depth, compared with the model without crustal eclogitization. During the continental subduction, the majority of the upper crustal materials are scraped off the downgoing continental slab to accrete in the collision zone, in accompany with obvious burial/exhumation processes (Figs. 8a and 8b). The remaining subducted upper crustal materials located in the lower part of the subduction channel are gradually detached from the slab at asthenospheric depths, indenting into the mantle wedge and forming a compositionally buoyant plume at the bottom of the overriding lithospheric mantle (Figs. 8a and 8d). In addition, the accumulation of highly radiogenic sediments and upper

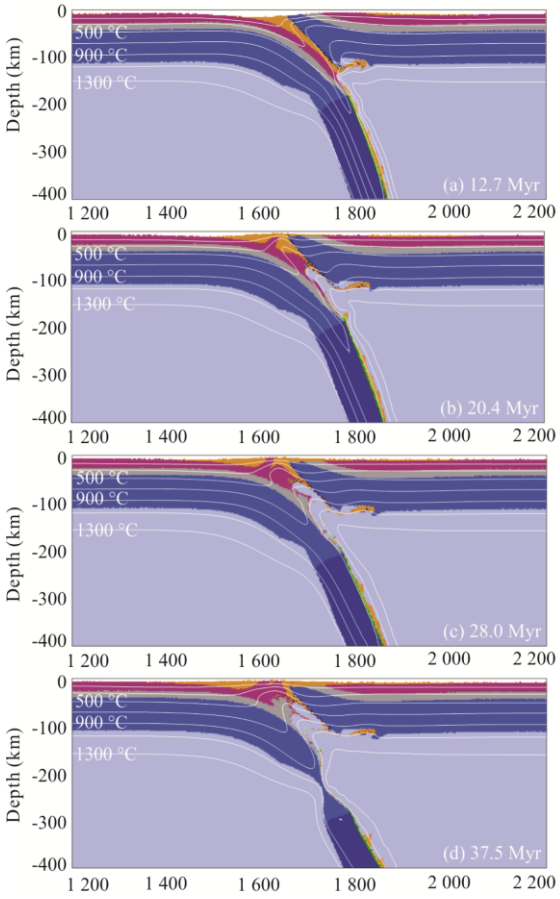

Figure 4. Evolution of the model without crustal eclogitization from initial continental collision to slab breakoff at time of (a) 12.7 Myr, (b) 20.4 Myr, (c) 28.0 Myr and (d) 37.5 Myr within an enlarged 1 000×400 km domain of the initial 2 800×1 400 km model. Colors of rocks are identical to those in Fig. 2. While numbered lines are isotherms in °C.

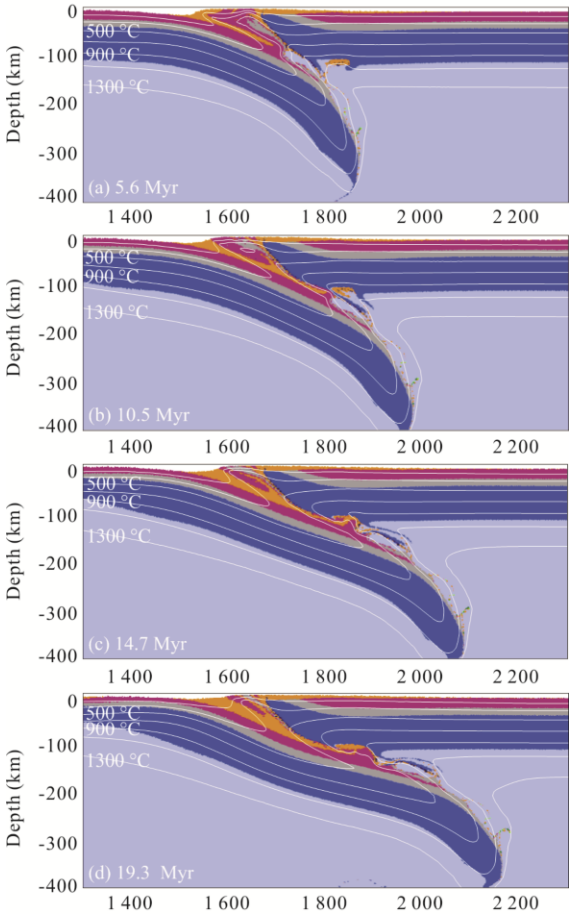

Figure 5. Evolution of the model without crustal eclogitization during continental subduction at time of (a) 5.6 Myr, (b) 10.5 Myr, (c) 14.7 Myr and (d) 19.3 Myr within an enlarged 1 000×400 km domain of the initial 2 800×1 400 km model. The end result of oceanic slab breakoff is used as the starting situation but with a pushing velocity of 4 cm/yr during this stage. Colors of rocks are identical to those in Fig. 2. While numbered lines are isotherms in °C.

continental crustal materials at the active margin, along with the strong shear heating due to continuous continental subduction, contribute to rising of isotherms in the accretionary wedge (Fig. 8d), which can greatly facilitate the crustal partial melting and thermal metamorphism. Eclogitization of the lower crust of the pro-continental plate not only makes the lower crust sink to a larger depth, but also causes a higher subduction angel during the pro-collisional stage.

3 DISCUSSION

3.1 Effects of Crustal Eclogitization on Subduction/Collision Dynamics

To first order, slab dynamics is regarded as a result of the balance of gravitational and hydrodynamic torque. The former tends to pull the slab downward, but the latter induces the slab to move upward to lower the subduction angle. Eclogitization of subducted oceanic crust and continental lower crust directly increases the average density and accordingly the gravitational torque of the subducting slab, which can make the slab sink deeply and steeply. On the basis of numerical results, effects of crustal eclogitization on plate dynamics are demonstrated in three different stages: oceanic subduction, oceanic slab breakoff, and continental subduction.

During oceanic subduction, the increasing slab pull force due to oceanic crustal eclogitization makes the slab subduct not only with an increasing dip angle but also with an increasing convergence velocity. After the initial continental collision, eclogitization of subducted oceanic crust and continental lower crust has a significant effect on the subsequent geodynamic evolution. Crustal eclogitization exerts a larger pull force on the subducting slab in comparison with that in the model without crustal eclogitization, and therefore greatly facilitates the rapid detachment of oceanic lithosphere from continental lithosphere. In this study, the duration time for slab breakoff after the initial continental collision in the model with crustal eclogitization is ~20 Myrs less than that in the model without crustal eclogitization (cf., Figs. 4 and 7). Moreover, in combination with eclogitization of continental lower crust, the pro-continental lithosphere can continuously sink to the asthenospheric depth, which at the same time increases the depth of slab breakoff (Fig. 7). In addition, as for the model without crustal eclogitization, oceanic slab breakoff is also accompanied with the large-scale exhumation of the subducted continental crust and subsequent strong upwelling of the hot asthenospheric materials through

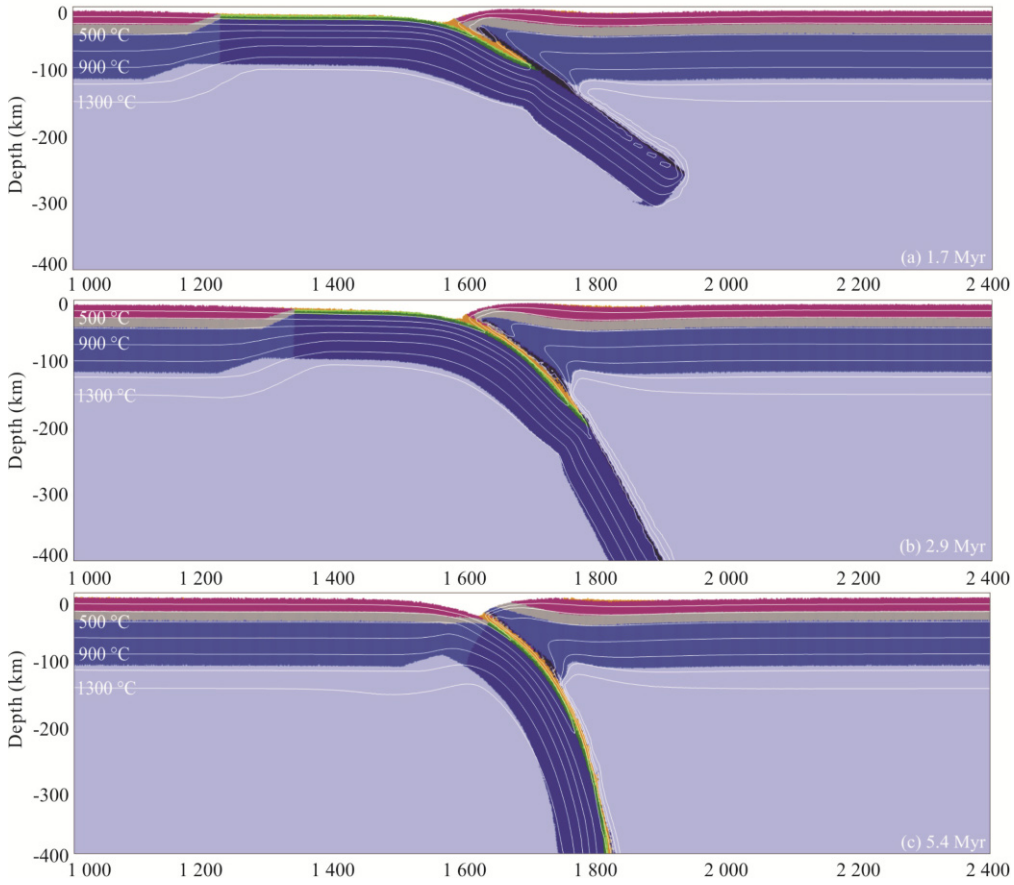

Figure 6. Evolution of the model with crustal eclogitization during oceanic subduction at time of (a) 1.7 Myr, (b) 2.9 Myr and (c) 5.4 Myr within an enlarged 1 400×400 km domain of the initial 2 800×1 400 km model. Colors of rocks are identical to those in Fig. 2. While numbered lines are isotherms in °C.

the gap between two plates (Fig. 4), which are also reflected in the topographic evolution. Mountain building keeps rather actively at this stage; especially around the time of slab breakoff, an abrupt large-scale uplift of the collision zone is recorded (Fig. 9a). Regarding the model with crustal eclogitization, deformation behaviour and topography of the collision zone is dominated by the downward sinking of the slab due to its negative buoyancy from the initial continental collision to slab breakoff and the corresponding orogenic process is inactive, even the topography around slab breakoff is relatively low and the orogen is narrow (Fig. 9b).

During continental subduction mainly driven by the pushing velocity assigned to the pro-continental plate, eclogitization of subducted continental lower crust exerts a downward pull force on the continental slab, which beneficially makes the pro-continental plate sink smoothly into the asthenosphere. Similar to the stage of oceanic subduction, crustal eclogitization during continental subduction not only significantly increases the subduction angle, causing the continental crustal materials to sink to a great depth, but also increases the convergence velocity attributed to the negative buoyancy of the eclogitized crustal materials. Topographic evolution during this stage is strongly correlated with the formation of accretionary wedge and deformation behaviour of the overriding continental plate (Fig. 9). The latter is greatly affected by the subduction angle. Specifically, a low subduction angle directly increases the length of the subduction channel and accordingly the shear stresses exerted on the overriding plate, which causes strong deformation of the overriding continent in the collision zone. The collisional area with an altitude of >1 000 m lengthens with continental subduction, and reaches ~400 km within ~20 Myrs in the model without crustal eclogitization (Fig. 9a); however, the collisional area almost keeps constant with a length of ~250 km during continental subduction under the condition of crustal eclogitization (Fig. 9b).

3.2 Thermal and Topography Evolution on the India-Asia Early Collision

It is generally accepted that the high and uniform elevation of the Tibetan plateau is caused by crustal thickening in response to India-Asia collision since the early Cenozoic (e.g., Searle et al., 2011; Hodges, 2000; Yin and Harrison, 2000). The plateau has been considered as the most prominent laboratory for exploring the continental collision mechanism (Molnar et al., 1993; Allegre et al., 1984) and climatic changes (Yao et al., 2013; Molnar et al., 1993). A large number of speculative hypotheses on the Tibetan evolution have been proposed, e.g., crustal shortening and thickening (England and Houseman, 1986), eastward strike-slip extrusions of SE Asia (Li et al., 2013; Tapponnier et al., 2001, 1982), underthrust of the Indian lithosphere beneath Asia (Li et al., 2011; Haines et al., 2003; DeCelles et al., 2002; Chemenda et al., 2000; Owens and Zandt, 1997; Powell, 1986; Klootwijk et al., 1985), destabilization and collapse of the tectonically thickened lithospheric root (Chung

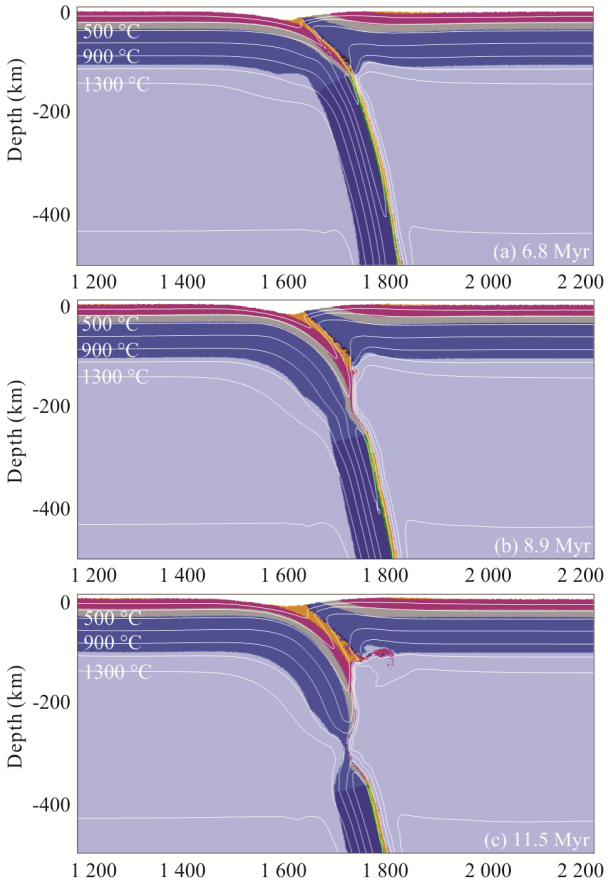

Figure 7. Evolution of the model with crustal eclogitization from initial continental collision to slab breakoff at time of (a) 6.8 Myr, (b) 8.9 Myr and (c) 11.5 Myr within an enlarged 1 000×500 km domain of the initial 2 800×1 400 km model. Colors of rocks are identical to those in Fig. 2. While numbered lines are isotherms in °C.

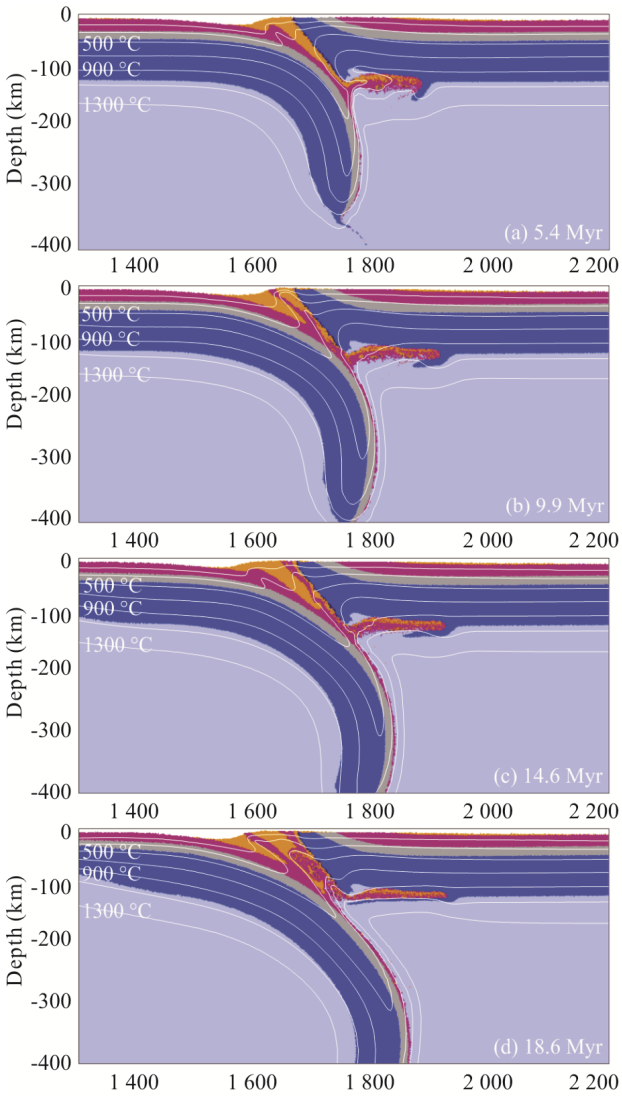

Figure 8. Evolution of the model with crustal eclogitization during continental subduction at time of (a) 5.4 Myr, (b) 9.9 Myr, (c) 14.6 Myr and (d) 18.6 Myr within an enlarged 700×400 km domain of the initial 2800×1400 km model. The end result of oceanic slab breakoff is used as the starting situation but with a pushing velocity of 4 cm/yr during this stage. Colors of rocks are identical to those in Fig. 2. While numbered lines are isotherms in °C.

et al., 2009, 2005; Platt and England, 1994; Houseman et al., 1981), northward crustal injection model (Chemenda et al., 2000; Zhao and Morgan, 1985), and southward subduction of the Asian lithosphere beneath Tibet (Paul et al., 2001; Roger et al., 2000; Willett and Beaumont, 1994). Recent geological, geophysical and geochemical studies suggest that the Tibetan Plateau possesses lateral variations of the subduction-related mantle structure (e.g., Chen Y et al., 2015; Chen L et al., 2013; Liang et al., 2012; Searle et al., 2011; Zhao W et al., 2011; Zhao J et al., 2010; Li et al., 2008; Yang et al., 2015) and temporal-spatial variations in post-collisional magmatism(e.g., Wang R et al., 2015; Zhang et al., 2014; Zhu et al., 2013; Chung et al., 2005, 2003; Ding et al., 2003), which indicate that the Tibetan Plateau might have been deformed through complex tectonic events.

According to our numerical models, during oceanic subduction, the downgoing slab experiences significant thermal- conduction heating, logically inducing dehydration of the hydrous minerals in the slab and partial melting of the subducted slab. Subsequently, partial melting of the overriding metasomatic mantle induces extensive magmatism, which will gradually move upward into the overriding crust resulting in the development of abundant crust-derived rocks, as observed in South Tibet (Zhu et al., 2013; Chung et al., 2005). Following the closure of the ocean basin, continental collision commences and the oceanic slab is subsequently detached from the pro-continental lithosphere. However, the duration time from the initial continental collision to slab breakoff depends on the slab pull force. Numerical results indicate that eclogitization of subducted crustal materials can greatly decrease this duration time but increase the breakoff depth at the same time. In addition, no matter whether the model contains crust eclogitization or not, oceanic slab breakoff can significantly promote exhumation of the subducted continental crustal materials and asthenospheric upwelling, inducing a considerable heating in the collision zone. Our numerical results reasonably explain the flare-ups of the Gangdese igneous rocks in South Lhasa and rapid exhumation of the subducted continental crust at ~50 Ma

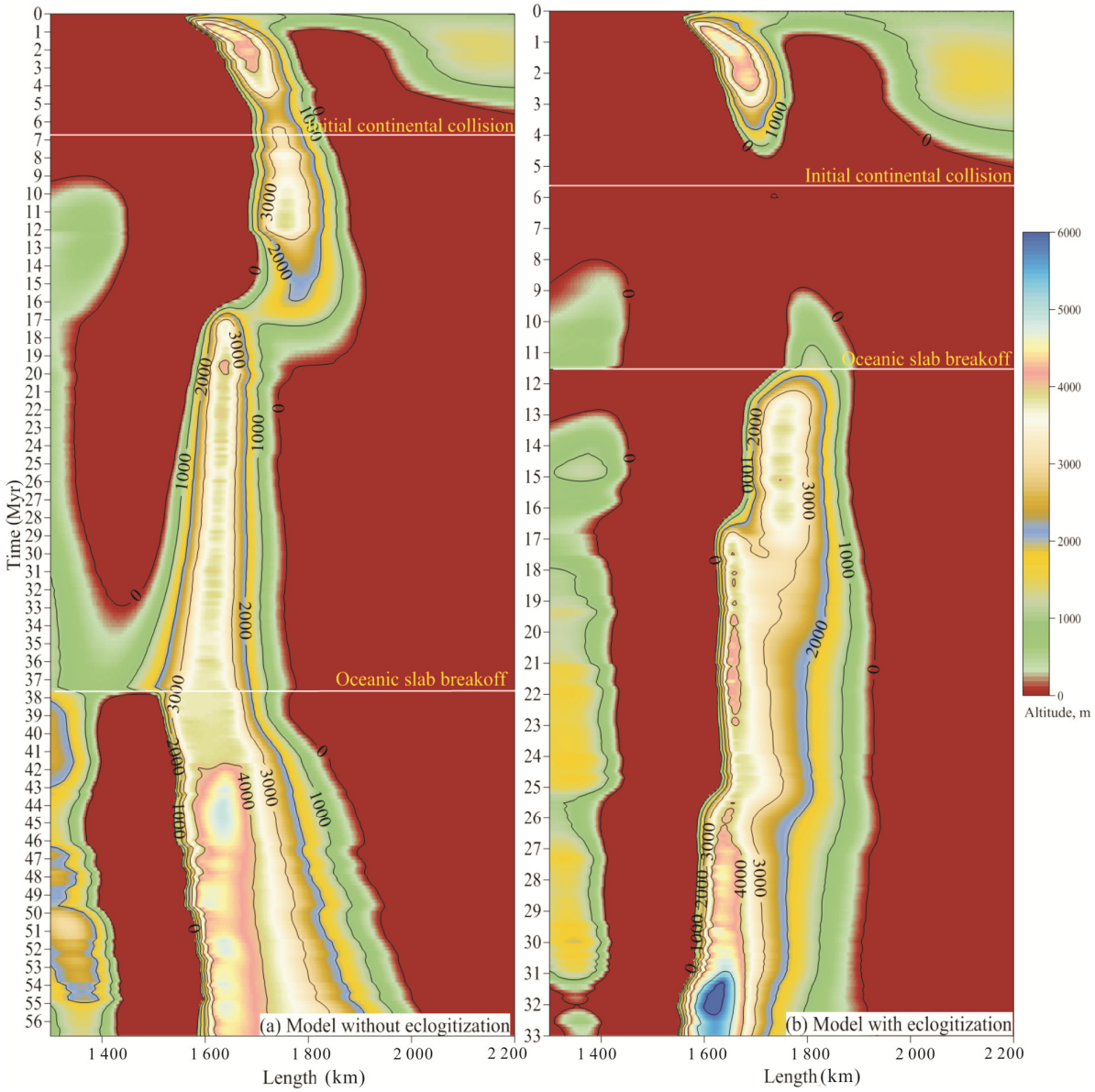

Figure 9. Topographic evolution of (a) model without crustal eclogitization and (b) model with crustal eclogitization. Times of initial continental collision and oceanic slab breakoff are marked.

in response to the slab breakoff (Wang Y et al., 2015, 2014; Chung et al., 2005). Meanwhile, the altitude of the collision zone can sharply increase by ~1 000 m in response to the slab breakoff (Fig. 9). The result indicates that the oceanic slab breakoff would lead to a substantial amount of topographic uplift in southern Tibet, similar to that proposed by Chung et al. (2005).

During continental subduction, the slab dip angle is closely correlated with eclogitization of subducted continental lower crust, which regulate the slab average density and the slab buoyancy nature. Thus, it is possible that the lateral variations of the eclogitization degree of the subducted Indian crust might to some extent contribute to the lateral variations of subduction angel along the Himalayan orogenic belt (Chen et al., 2015; Li et al., 2008). When crustal eclogitization takes place hardly or incompletely, the pro-continental plate will subduct shallowly, as shown in Fig. 5. Under this condition, the shallow continental slab squeezes part of the hot asthenospheric materials out of the mantle wedge, subsequently cooling the overriding lithospheric mantle. Such scenario might account for the relatively rare igneous activity at ~30–50 Ma in South Tibet. In addition, this process also illustrates the building of the Himalaya, attributed to the combined effects of lateral accretion of the scraped Indian continental crustal materials and upwarping of the overriding plate, the high-grade metamorphism in the accretionary wedge and rapidly widespread exhumation of the Indian crustal materials (Yin, 2006). However, as a relatively simplified pre- and post-continental collision model without consideration of long term complicated and evolving tectonic activity, our mode results can only provide limited implications for topographic evolution of the Tibetan Plateau during the post-collisional stage.

4 CONCLUSION

In this study, the sensitivity tests of model predictions to crustal eclogitization are evaluated. Effects of eclogitization of

subducted oceanic crust and continental lower crust are investigated at three successive stages of oceanic subduction, slab breakoff, and continental subduction, respectively. Crustal eclogitization directly increases the average slab density and the net slab pull force, causing the slab to subduct deeply and steeply. Numerical results demonstrate that the eclogitization of subducted crustal materials not only can greatly decrease the duration time from the initial continental collision to slab breakoff, but also can increase the breakoff depth. The detachment of oceanic slab from the pro-continental lithosphere is accompanied by rapid exhumation of the subducted continental crust and a sharp uplift of the collision zone, in response to disappearance of the downward drag force and the induced asthenospheric upwelling. During continental subduction, the slab dip angle is closely correlated with eclogitization of subducted continental lower crust, which influences the thermal and topographic evolution of the collision zone. Our numerical results provide important implications for the thermal and topographic evolution at the early stage of India-Asia collision. It is proposed that the lateral variations of the eclogitization degree of the subducted Indian crust might to some extent contribute to the lateral variations of subduction angel along the Himalayan orogenic belt.

ACKNOWLEDGMENTS

This study benefited from financial supports by the National Natural Science Foundation of China (Nos. 41490613, 41190073 and 41304071) and the National Basic Research Program of China (Nos. 2014CB440901 and 2015CB856106). Thorough and constructive reviews by two anonymous reviewers are much appreciated. The final publication is available at Springer via http://dx.doi.org/10.1007/s12583-016-0701-9.

REFERENCES CITED

Allegre, C. J., Courtillot, V., Tapponnier, P., et al., 1984. Structure and Evolution of the Himalaya-Tibet Orogenic Belt. *Nature*, 307(5946): 17–22

Bittner, D., Schmeling, H., 1995. Numerical Modeling of Melting Processes and Induced Diapirism in the Lower Crust. *Geophysical Journal International*, 123(1): 59–70

Chemenda, A. I., Burg, J. P., Mattauer, M., 2000. Evolutionary Model of the Himalaya-Tibet System: Geopoem Based on New Modelling, Geological and Geophysical Data. *Earth and Planetary Science Letters*, 174(3–4): 397–409

Chen, L., Gerya, T. V., Zhang, Z. J., et al., 2013. Formation Mechanism of Steep Convergent Intracontinental Margins: Insights from Numerical Modeling. *Geophysical Research Letters*, 40(10): 2000–2005

Chen, Y., Li, W., Yuan, X., et al., 2015. Tearing of the Indian Lithospheric Slab beneath Southern Tibet Revealed by SKS-Wave Splitting Measurements. *Earth and Planetary Science Letters*, 413: 13–24

Chung, S. L., Liu, D. Y., Ji, J. Q., et al., 2003. Adakites from Continental Collision Zones: Melting of Thickened Lower Crust Beneath Southern Tibet. *Geology*, 31(11): 1021–1024

Chung, S. L., Chu, M. F., Ji, J., et al., 2009. The Nature and Timing of Crustal Thickening in Southern Tibet: Geochemical and Zircon Hf Isotopic Constraints from Post-collisional Adakites. *Tectonophysics*, 477(1): 36–48

Chung, S. L., Chu, M. F., Zhang, Y., et al., 2005. Tibetan Tectonic Evolution Inferred from Spatial and Temporal Variations in Post-collisional Magmatism. *Earth Science Reviews*, 68(3): 173–196

Clauser, C., Huenges, E., 1995. Thermal Conductivity of Rocks and Minerals. *AGU Reference Shelf*, 3: 105–126

DeCelles, P. G., Robinson, D. M., Zandt, G., 2002. Implications of Shortening in the Himalayan Fold-Thrust Belt for Uplift of the Tibetan Plateau. *Tectonics*, 21(6): TC1062

Ding, L., Kapp, P., Zhong, D. L., et al., 2003. Cenozoic Volcanism in Tibet: Evidence for a Transition from Oceanic to Continental Subduction. *Journal of Petrology*, 44(10): 1833–1865

Duesterhoeft, E., Quinteros, J., Oberhansli, R., et al., 2014. Relative Impact of Mantle Densification and Eclogitization of Slabs on Subduction Dynamics: A Numerical Thermodynamic/Thermokinematic Investigation of Metamorphic Density Evolution. *Tectonophysics*, 637: 20–29

England, P., Houseman, G., 1986. Finite Strain Calculations of Continental Deformation. 2. Comparison with the India- Asia Collision Zone. *Journal of Geophysical Research*: *Solid Earth and Planets*, 91(B3): 3664–3676

Forsyth, D., Uyeda, S, 1975. On the Relative Importance of the Driving Forces of Plate Motion. *Geophysical Journal International*, 43(1): 163–200.

Gerya, T. V., 2010, Introduction to Numerical Geodynamic Modelling. Cambridge University Press, New York. 345

Gerya, T. V., Yuen, D. A., 2003. Characteristics-Based Marker-in-Cell Method with Conservative Finite-differences Schemes for Modeling Geological Flows with Strongly Variable Transport Properties. *Physics of the Earth and Planetary Interiors*, 140(4): 293–318

Giunchi, C., Ricard, Y., 1999. High-Pressure/ Low-Temperature Metamorphism and the Dynamics of an Accretionary Wedge. *Geophysical Journal International*, 136(3): 620–628

Haines, S. S., Klemperer, S. L., Brown, L., et al., 2003. INDEPTH III Seismic Data: From Surface Observations to Deep Crustal Processes in Tibet. *Tectonics*, 22(1): 1001. doi:10.1029/2001TC001305

Hodges, K. V., 2000. Tectonics of the Himalaya and Southern Tibet from Two Perspectives. *Geological Society of America Bulletin*, 112(3): 324–350

Houseman, G. A., Mckenzie, D. P., Molnar, P., 1981. Convective Instability of a Thickened Boundary-Layer and Its Relevance for the Thermal Evolution of Continental Convergent Belts. *Journal of Geophysical Research*, 86(Nb7): 6115–6132

Jischke, M. C., 1975. Dynamics of Descending Lithospheric Plates and Slip Zones. *Journal of Geophysical Research*, 80(35): 4809–4813

Klootwijk, C. T., Conaghan, P. J., Powell, C. M., 1985. The Himalayan Arc-Large-Scale Continental Subduction,

Oroclinal Bending and Back-Arc Spreading. *Earth and Planetary Science Letters*, 75: 167–183

Leech, M. L., 2001. Arrested Orogenic Development: Eclogitization, Delamination, and Tectonic Collapse. *Earth and Planetary Science Letters*, 185(1–2): 149–159

Li, C., van der Hilst, R. D., Meltzer, A. S., et al., 2008. Subduction of the Indian Lithosphere Beneath the Tibetan Plateau and Burma. *Earth and Planetary Science Letters*, 274: 157–168

Li, Z. H., Xu, Z. Q., Gerya, T. V., 2011. Flat Versus Steep Subduction: Contrasting Modes for the Formation and Exhumation of High- to Ultrahigh-Pressure Rocks in Continental Collision Zones. *Earth and Planetary Science Letters*, 301: 65–77

Li, Z. H., 2014. A Review on the Numerical Geodynamic Modeling of Continental Subduction, Collision and Exhumation. *Science China*: *Earth Sciences*, 57: 47–69

Li, Z. H., Xu, Z. Q., Gerya, T. V., et al., 2013. Collision of Continental Corner from 3-D Numerical Modeling. *Earth and Planetary Science Letters*, 380: 98–111

Liang, X., Sandvol, E., Chen, Y. J., et al., 2012. A Complex Tibetan Upper Mantle: A Fragmented Indian Slab and no South-Verging Subduction of Eurasian Lithosphere. *Earth and Planetary Science Letters*, 333: 101–111

Lithgow-Bertelloni, C., Richards, M. A., 1995. Cenozoic Plate Driving Forces. *Geophysical Research Letters*, 22(11): 1317–1320

Lustrino, M., 2005. How the Delamination and Detachment of Lower Crust can Influence Basaltic Magmatism. *Earth-Science Reviews*, 72: 21–38

Manea, V., Manea, M., Kostoglodov, V., et al., 2006. Intraslab Seismicity and Thermal Stress in the Subducted Cocos Plate Beneath Central Mexico. *Tectonophysics*, 420: 389–408

Molnar, P., England, P., Martinod, J., 1993. Mantle Dynamics, Uplift of the Tibetan Plateau, and the Indian Monsoon. *Reviews of Geophysics*, 31(4): 357–396

Owens, T. J., Zandt, G., 1997. Implications of Crustal Property Variations for Models of Tibetan Plateau Evolution. *Nature*, 387(6628): 37–43

Paul, J., Burgmann, R., Gaur, V. K., et al., 2001. The Motion and Active Deformation of India. *Geophysical Research Letters*, 28: 647–650

Platt, J. P., England, P. C., 1994. Convective Removal of Lithosphere beneath Mountain Belts—Thermal and Mechanical Consequences. *American Journal of Science*, 294(3): 307–336

Powell, C. M., 1986. Continental Underplating Model for the Rise of the Tibetan Plateau. *Earth and Planetary Science Letters*, 81: 79–94

Ranalli, G., 1995. Rheology of the Earth. Springer, Netherlands. 414

Riedell, M. R., Karato, S., 1996. Microstructural Development during Nucleation and Growth. *Geophysical Journal International*, 125(2): 397–414

Roger, F., Tapponnier, P., Arnaud, N., et al., 2000. An Eocene Magmatic Belt across Central Tibet: Mantle Subduction Triggered by the Indian Collision? *Terra Nova*, 12: 102–108

Schellart, W. P., 2004. Quantifying the Net Slab Pull Force as a Driving Mechanism for Plate Tectonics. *Geophysical Research Letters*, 31(7): L07611. doi: 10.1029/2004GL019528

Searle, M. P., Elliott, J., Phillips, R., et al., 2011. Crustal–Lithospheric Structure and Continental Extrusion of Tibet. *Journal of the Geological Society*, 168: 633–672

Stevenson, D. J., Turner, J. S., 1977. Angle of Subduction. *Nature*, 270: 334–336

Tapponnier, P., Peltzer, G., Ledain, A. Y., et al., 1982. Propagating Extrusion Tectonics in Asia—New Insights from Simple Experiments with Plasticine. *Geology*, 10(12): 611–616

Tapponnier, P., Xu, Z. Q., Roger, F., et al., 2001. Oblique Stepwise Rise and Growth of the Tibet Plateau. *Science*, 294(5547): 1671–1677

Turcotte, D. L., Schubert, G., 2002. Geodynamics. Cambridge University Press, Cambridge. 636

van Hinsbergen, D. J. J., Steinberger, B., Doubrovine, P. V., et al., 2011. Acceleration and Deceleration of India-Asia Convergence since the Cretaceous: Roles of Mantle Plumes and Continental Collision. *Journal of Geophysical Research*: *Solid Earth*, 116: B06101

van Hunen, J., van den Berg, A. P., Vlaar, N. J., 2001. Latent Heat Effects of the Major Mantle Phase Transitions on Low-Angle Subduction. *Earth and Planetary Science Letters*, 190: 125–135

van Hunen, J., van den Berg, A. P., Vlaar, N. J., 2004. Various Mechanisms to Induce Present-day Shallow Flat Subduction and Implications for the Younger Earth: A Numerical Parameter Study. *Physics of the Earth and Planetary Interiors*, 146: 179–194

Vigny, C., Ricard, Y., Froidevaux, C., 1991. The Driving Mechanism of Plate Tectonics. *Tectonophysics*, 187(4): 345–360

Wang, R., Richards, J. P., Zhou, L. M., et al., 2015. The Role of Indian and Tibetan Lithosphere in Spatial Distribution of Cenozoic Magmatism and Porphyry Cu-Mo Deposits in the Gangdese Belt, Southern Tibet. *Earth Science Reviews*, 150: 68–94

Wang, Y., Li, S., Ma, L., et al., 2015. Geochronological and Geochemical Constraints on the Petrogenesis of Early Eocene Metagabbroic Rocks in Nabang (SW Yunnan) and Its Implications on the Neotethyan Slab Subduction. *Gondwana Research*, 27(4): 1474–1486

Wang, Y., Zhang, L., Cawood, P. A., et al., 2014. Eocene Supra-Subduction Zone Mafic Magmatism in the Sibumasu Block of SW Yunnan: Implications for Neotethyan Subduction and India-Asia Collision. *Lithos*, 206: 384–399

Willett, S. D., Beaumont, C., 1994. Subduction of Asian Lithospheric Mantle beneath Tibet Inferred from Models of Continental Collision. *Nature*, 369(6482): 642–645

Yao, T. D., Masson-Delmotte, V., Gao, J., et al., 2013. A Review of Climatic Controls on $\delta^{18}O$ in Precipitation over the Tibetan Plateau: Observations and Simulations. *Reviews of Geophysics*, 51(4): 525–548

Yang, J. Z., Liu, X. C., Wu, Y. B., et al., 2015. Zircon Record of Ocean-Continent Subduction Transition Process of Dulan UHPM Belt, North Qaidam. Journal of Earth Science, 26(5): 617–625. doi:10.1007/s12583-015-0585-0

Yin, A., Harrison, T. M., 2000. Geologic Evolution of the Himalayan-Tibetan Orogen. *Annual Review of Earth and Planetary Sciences*, 28(1): 211–280

Yin, A., 2006. Cenozoic Tectonic Evolution of the Himalayan Orogen as Constrained by Along-Strike Variation of Structural Geometry, Exhumation History, and Foreland Sedimentation. *Earth Science Reviews*, 76: 1–131

Zhang, Z. M., Dong, X., Santosh, M., et al., 2014. Metamorphism and Tectonic Evolution of the Lhasa Terrane, Central Tibet. *Gondwana Research*, 25: 170–189

Zhao, J., Yuan, X., Liu, H., et al., 2010. The Boundary between the Indian and Asian Tectonic Plates below Tibet. *Proceedings of the National Academy of Sciences*, 107: 11229–11233

Zhao, W. L., Morgan, W. J., 1985. Uplift of Tibetan Plateau. *Tectonics*, 4(4): 359–369

Zhao, W., Kumar, P., Mechie, J., et al., 2011. Tibetan Plate Overriding the Asian Plate in Central and Northern Tibet. *Nature Geoscience*, 4: 870–873

Zheng, Y. F., Zhao, Z. F., Chen, Y. X., 2013. Continental Subduction Channel Processes: Plate Interface Interaction during Continental Collision. *Chinese Science Bulletin*, 58(35): 4371–4377

Zhu, D. C., Zhao, Z. D., Niu, Y., et al., 2013. The Origin and Pre-Cenozoic Evolution of the Tibetan Plateau. *Gondwana Research*, 23: 1429–1454